Journal of Applied Physics ARTICLE pubs.aip.org/aip/jap

The transition between the collision-dominated and ballistic electron transport regimes as the device length is reduced: A continuum analysis

Cite as: J. Appl. Phys. **136**, 035702 (2024); doi: 10.1063/5.0211046
Submitted: 28 March 2024 · Accepted: 17 June 2024 ·
Published Online: 16 July 2024

Alireza Azimi,[1] Mohammadreza Azimi,[1] Michael S. Shur,[2] and Stephen K. O'Leary[1,a)]

AFFILIATIONS

[1]School of Engineering, The University of British Columbia, Kelowna, British Columbia V1V 1V7, Canada
[2]Electrical, Computer, and Systems Engineering, Rensselaer Polytechnic Institute, Troy, New York 12110, USA

[a)]**Author to whom correspondence should be addressed:** stephen.oleary@ubc.ca

ABSTRACT

Noting that the conventional collision-dominated electron transport perspective is only relevant when the length scale over which the transit occurs is greater than the electron's mean free path, one can conceptually partition the electron transport "space" into collision-dominated and ballistic electron transport regimes. As the boundaries between these regimes are quite porous, in this analysis, we devise a means of quantitatively examining the transition between electron transport regimes as the length scale is reduced on a continuum basis. Our approach introduces a collision-dominated fractional scattering parameter, this parameter quantifying the fraction of the total scattering rate that arises purely from bulk scattering processes, contact scattering also contributing to the total scattering rate. We pursue this analysis for two conventional semiconductors of interest, silicon and gallium arsenide. A determination of the dependence of the results on both the length scale and the crystal temperature is pursued. Finally, for the specific case of room temperature, a comparison with the results of experiment is performed.

I. INTRODUCTION

The remarkable advances that have occurred within microelectronics have primarily been achieved through the adoption of a feature-length scale reduction strategy.[1–4] Prompted by Moore's law, this scaling approach to technological progress has served the needs of the microelectronics industry since its genesis.[5,6] Unfortunately, with the projected scale limit of silicon (Si)-based technologies about to be realized, there is a widespread recognition within the community that new approaches for technological advancement must be sought if development within the field is to continue apace.[7] In recognition of this critical challenge, in recent years, a plethora of alternate materials and novel device configurations have been contemplated, very short gate lengths being realized in a number of non-Si-based material systems. Recent successes have included the fabrication of nanometer-scale gate lengths in carbon nanotube and molybdenum disulfide-based transistors.[8,9]

It is widely recognized that the nature of electron transport changes with the length scale over which the transport occurs. Shur and Eastman[10] note, for example, that the conventional collision-dominated based electron transport perspective is only relevant when the length scale, L, is long when contrasted with the mean free path of an electron, λ. When L is shorter than λ, the electrons transiting a device will not have the time required in order to achieve steady-state. Accordingly, they will behave ballistically. When an electron experiences ballistic electron transport, following in the tradition of Kastalsky *et al.*[11,12] and others,[13] Dmitriev and Shur[14] have found it instructive to introduce the concept of ballistic mobility, $\mu_{\text{ball.}}$, which reflects the impact of scattering that only occurs at the device boundaries, i.e., the contacts; if an electron experiences true ballistic transport, no other scattering will be experienced by the electron as it transits the device. Through the use of a Matthiessen's-rule based approach, an effective mobility, $\mu_{\text{eff.}}$, can be determined through a combination of $\mu_{\text{ball.}}$ and the conventional collision-dominated based mobility, μ_{bulk}, i.e., the bulk mobility.

Conceptually, the electron transport "space" can be partitioned into two distinct electron transport categories, i.e., a collision-dominated

electron transport regime and a ballistic electron transport regime, based on whether the length scale, L, is longer or shorter than the electron's mean free path, λ, respectively, the electron transport "space" being visually represented using the simplified electron transport regime classification diagram depicted in Fig. 1; a further segmentation of the electron transport "space" based on the relevant screening length, L_D, initially suggested by Lee and Shur,[15] was recently pursued by Azimi *et al.*[16] Through an evaluation of the mean free path for a number of representative electronic materials of interest, the analysis of Azimi *et al.*[16] offers a quantitative means of delineating between the collision-dominated and ballistic electron transport regimes. Noting that the two electron transport regime categories shown in Fig. 1 are in actual fact quite porous, i.e., that some of the electrons with L greater than λ behave ballistically and that some of the electrons with L less than λ experience collisions, we aim to go beyond the conceptual electron transport "space" duopoly embodied in Fig. 1 and develop a means of quantitatively examining the transition between the various electron transport regimes.

We cast the analysis within the framework of the scattering formalism of Chilleri *et al.*,[17,18] this formalism allowing for the two electron transport regimes to be placed on a continuum rather than the abrupt electron transport "space" partition embodied in Fig. 1. To make the analysis concrete, we will pursue it for two conventional semiconductors of interest, Si and gallium arsenide (GaAs), noting that the analysis could equally well be applied to more exotic materials. To simplify the analysis, we will assume intrinsic materials, i.e., the complete absence of impurities for both cases. We employ a two-dimensional analysis of the electron transport, this being representative of that experienced by an electron in the neighborhood of a two-dimensional electron gas (2DEG).[19] A determination of the dependence of the results on both the length scale, L, and the crystal temperature, T, is sought. To simplify matters even further, we pursue results in the non-degenerate limit. For the specific case of room temperature, a comparison with the results of experiment is performed for the two materials under consideration.

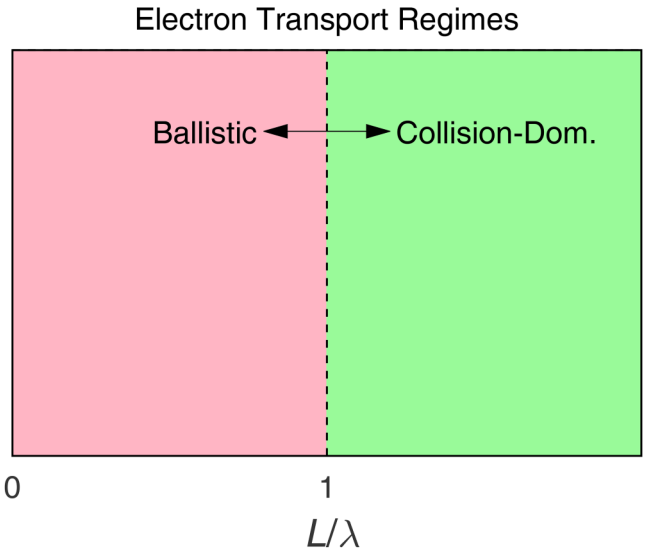

FIG. 1. A simplified electron transport regime classification diagram. In this diagram, the electron transport "space" is partitioned into two regimes, a collision-dominated electron transport regime and a ballistic electron transport regime, based on whether the length scale, L, is larger or smaller than the electron's mean free path, λ, respectively. An enriched version of this constellation diagram, which further segments the electron transport "space" into two additional categories, is provided in Fig. 1 of Azimi *et al.*[16] The online version of this figure is depicted in color.

This paper is organized in the following manner. In Sec. II, the electron transport formalism that underpins the analysis is introduced. Evaluations of the temperature dependence of various relevant mobilities are then presented in Sec. III. In Sec. IV, the dependence of the effective mobility on the length scale, L, and the temperature, T, is then determined. The introduction and evaluation of a parameter that quantifies the fraction of the total scattering rate that arises from bulk scattering processes is also featured in Sec. IV. For the specific case of room temperature, a comparison with the results of experiment for the dependence of the effective mobility on the length scale, L, is then discussed in Sec. V for the two materials under consideration. Finally, the conclusions of this analysis are drawn in Sec. VI.

II. FORMALISM

The recently developed scattering formalism of Chilleri *et al.*[17,18] treats the total scattering rate, λ_{tot}, as the sum over the scattering rates associated with the individual scattering processes. If $\lambda^{(i)}$ corresponds to the scattering rate associated with the i-th scattering process, then it follows that

$$\lambda_{tot} = \sum_i \lambda^{(i)}. \tag{1}$$

Recalling that the mobility of an electron within a given material may be written as

$$\mu = \frac{q\,\tau}{m^*}, \tag{2}$$

where q represents the electron charge, m^* denotes the electron effective mass, and τ corresponds to the momentum relaxation time, if we interpret the reciprocal of $\lambda^{(i)}$ as being the momentum relaxation time associated with this i-th scattering process, a mobility associated with the i-th scattering process, $\mu^{(i)}$, can thus be defined, i.e.,

$$\mu^{(i)} \equiv \frac{q}{m^*\,\lambda^{(i)}}, \tag{3}$$

where all terms in Eq. (3) are as previously defined. If we further interpret τ as corresponding to the reciprocal of the total scattering rate, i.e.,

$$\mu = \frac{q}{m^*\,\lambda_{tot}}, \tag{4}$$

then from Eqs. (1), (3), and (4), it can be shown that

$$\frac{1}{\mu} = \sum_i \frac{1}{\mu^{(i)}}, \tag{5}$$

which is essentially a form of Matthiessen's rule.

An examination of the dependence of the mobility of a given sample on its length scale, L, is instructive; following in the tradition of Kastalsky *et al.*,[11,12] by length scale we are referring to the length of a given semiconductor sample, this length scale serving as a proxy for the path length that an electron must traverse across a device fabricated from such a sample. In order to treat the transition from the collision-dominated to ballistic electron transport regimes as the length scale, L, is reduced, we draw upon this formalism of Chilleri *et al.*,[17,18] adding contact scattering to the bulk scattering processes. Accordingly, within the scope of Eq. (1), the total scattering rate may be expressed as the sum over the contact scattering rate, $\lambda_{\text{cont.}}$, and the bulk scattering rate, λ_{bulk}, i.e.,

$$\lambda_{\text{tot}} = \lambda_{\text{cont.}} + \lambda_{\text{bulk}}, \tag{6}$$

where λ_{bulk} may, in turn, be expressed as a sum over the various bulk scattering rates, i.e.,

$$\lambda_{\text{bulk}} = \sum_i \lambda^{(i)}. \quad \text{(bulk only)} \tag{7}$$

Noting that contact scattering processes dominate for short L, i.e., the distance across the sample is so short that the electrons will have completed their transit and scattered at the sample boundaries (contacts) long before bulk scattering processes have effect, Dmitriev and Shur[14] introduced a mobility associated with this contact scattering,

$$\mu_{\text{ball.}} = \alpha \frac{q\,L}{m^*\,v}, \tag{8}$$

where α is a coefficient of the order of unity; for short L, assuming "hard" contacts, i.e., each time an electron reaches the device boundary (contact) it scatters, τ will correspond to the transit time across the sample, this time corresponding to the length scale, L, divided by a representative velocity, v, the α factor arising from the ensemble and geometrical averaging that must be performed. Note that $\lambda_{\text{cont.}}$ and λ_{bulk} may be determined from $\mu_{\text{ball.}}$ and μ_{bulk}, respectively, i.e., through the use of Eq. (3),[20–23]

$$\lambda_{\text{cont.}} = \frac{q}{m^*\,\mu_{\text{ball.}}} \tag{9}$$

and

$$\lambda_{\text{bulk}} = \frac{q}{m^*\,\mu_{\text{bulk}}}. \tag{10}$$

We seek a determination of the dependence of the effective mobility, $\mu_{\text{eff.}}$, on the length scale, L. Following from Eq. (5), for a sample of length scale, L, one can obtain a relationship between the effective mobility, $\mu_{\text{eff.}}$, the ballistic mobility, $\mu_{\text{ball.}}$, and the bulk mobility, μ_{bulk}, i.e.,

$$\frac{1}{\mu_{\text{eff.}}} = \frac{1}{\mu_{\text{ball.}}} + \frac{1}{\mu_{\text{bulk}}}, \tag{11}$$

where from Eqs. (3), (7), and (10), it can be seen that the evaluation of μ_{bulk} itself corresponds to the sum over all of the aforementioned bulk scattering process related mobilities, i.e.,

$$\frac{1}{\mu_{bulk}} = \sum_i \frac{1}{\mu^{(i)}}, \quad \text{(bulk only)} \tag{12}$$

all the terms in Eqs. (11) and (12) being as defined earlier; a similar approach was employed by Chilleri *et al.*[24] It is noted that in the short length scale limit, i.e., as $L \to 0$, that $\mu_{\text{ball.}}$ becomes quite small, and thus, it dominates the evaluation of Eq. (11), i.e., $\mu_{\text{eff.}} \to \mu_{\text{ball.}}$. In contrast, for the long length scale limit, i.e., as $L \to \infty$, that $\mu_{\text{ball.}}$ becomes quite large, and thus, it becomes insignificant in the evaluation of Eq. (11), i.e., $\mu_{\text{eff.}} \to \mu_{\text{bulk}}$. Equation (11) provides the analytical framework for the subsequent analysis.

III. BALLISTIC AND BULK MOBILITY EVALUATIONS

We start the analysis with an evaluation of the dependence of the $\mu_{\text{ball.}}$ on the temperature, T. From Eq. (8) it is seen that $\mu_{\text{ball.}}$ linearly increases with the length scale, L, v for the non-degenerate case being set to the thermal velocity, $v_{\text{th.}}$. For the case of two-dimensional electron transport, it can be shown that

$$v_{\text{th.}} = \sqrt{\frac{\pi k_B T}{2m^*}}, \tag{13}$$

where k_B represents the Boltzmann constant, m^* and T being as defined earlier; see the Appendix. As we are considering the case of two-dimensional electron transport, following the lead of Dmitriev and Shur,[14] we set $\alpha = \frac{1}{2}$. For the two materials being considered in this analysis, with the effective mass values set as indicated in Table I, the dependence of $\mu_{\text{ball.}}$ on T is depicted in Fig. 2 for two representative length scales, these spanning over the range of values considered reasonable. It is noted that as the effective mass associated with GaAs is smaller than that associated with Si (by a factor of about three), in all cases the ballistic mobility associated with GaAs exceeds that associated with Si by the square-root of the same factor.

Owing to the important role that μ_{bulk} plays in shaping $\mu_{\text{eff.}}$, it is instructive to compare the temperature dependence of $\mu_{\text{ball.}}$ with

TABLE I. The effective mass, m^*, for the two materials considered in this analysis, m_e representing the free electron mass.

Material	m^*
Si	0.19 m_e
GaAs	0.063 m_e

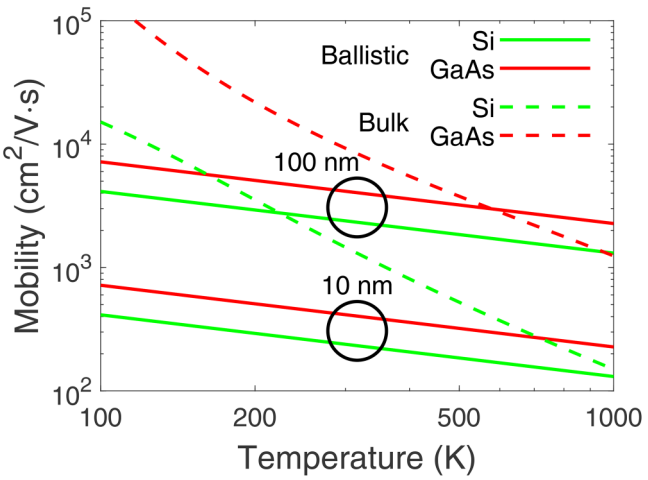

FIG. 2. The temperature dependence of the ballistic mobility, $\mu_{ball.}$, for a variety of length scale selections, for the cases of Si and GaAs. The corresponding bulk mobility, μ_{bulk}, temperature dependencies are also shown. The online version of this figure is depicted in color.

the corresponding temperature dependence of the bulk mobility, μ_{bulk}. Accordingly, in Fig. 2, we also plot the temperature dependencies of the bulk Si and bulk GaAs mobilities. For the case of bulk Si, we recreate and extend the low-field mobility results of Rode[25] over the temperature range of 100–1000 K (Rode[25] did not present results corresponding to all of the relevant bulk scattering processes considered in their analysis over the entire range of temperatures considered by us, hence the need for an extension in the results over a broader range of temperatures); for the case of intrinsic Si, Rode[25] considers just the bulk mobility contributions ascribed to the intervalley and the acoustic deformation potential scattering processes, $\mu_{int.}$ and $\mu_{ac.}$, respectively, so from Eq. (12), it can be seen that

$$\frac{1}{\mu_{bulk}} = \frac{1}{\mu_{int.}} + \frac{1}{\mu_{ac.}}. \tag{14}$$

For the case of GaAs, however, we performed all of the calculations from scratch using the analytical framework of Shur *et al.*,[26] our results being imperceptibly distinct from other GaAs results found in the literature; for the case of intrinsic GaAs, Shur *et al.*[26] considers just the bulk mobility contributions ascribed to the polar optical and acoustic deformation potential bulk scattering processes, $\mu_{pol.}$ and $\mu_{ac.}$, respectively, so from Eq. (12), it can be seen that

$$\frac{1}{\mu_{bulk}} = \frac{1}{\mu_{pol.}} + \frac{1}{\mu_{ac.}}. \tag{15}$$

It should be noted that on account of these materials being intrinsic, a number of otherwise important bulk scattering processes have been neglected in this analysis, such as the ionized impurity and the piezoelectric scattering processes. It is interesting to note that while $\mu_{ball.}$ follows a $T^{-1/2}$ temperature dependence [recall the combination of Eqs. (8) and (13)], the bulk mobility, μ_{bulk}, seems to follow a much stronger temperature dependence, for both Si and GaAs. The fact that intercepts of $\mu_{ball.}$ and μ_{bulk} occur at different temperatures for the cases of Si and GaAs suggests that the role of the collision-dominated and ballistic electron transport regimes will be distinct for each material.

IV. EFFECTIVE MOBILITY AND COLLISION-DOMINATED FRACTIONAL SCATTERING PARAMETER EVALUATIONS

Building upon this theoretical infrastructure, we continue the analysis with an evaluation of the dependence of the effective mobility, $\mu_{eff.}$, on both the length scale, L, and the crystal temperature, T, for the two materials considered in this analysis. For the purposes of this analysis, the temperature dependence of μ_{bulk} is set to that shown in Fig. 2. The effective mobility, $\mu_{eff.}$, is determined through the use of Eq. (11), $\mu_{ball.}$ being determined through the use of Eqs. (8) and (13), m^* being set to the values prescribed in Table I. The results are depicted in Figs. 3(a) and 3(b) for the cases of Si and GaAs, respectively. We first note that, for both cases, $\mu_{eff.}$ diminishes as L shortens, the small $\mu_{ball.}$ values corresponding to small L undoubtedly being the dominant factor responsible for this transition. We also note that for a set value of L, an increase in the crystal temperature results in a decrease in $\mu_{eff.}$, this arising from the decreases in $\mu_{ball.}$ and μ_{bulk} observed in Fig. 2. An examination of the dependence of $\mu_{eff.}$ at the extremes of L is instructive. For the shortest length scale selections, i.e., for L set to 10 nm, the electron transport is dominated by the ballistic mobility, $\mu_{ball.}$, $\mu_{eff.}$ essentially following $\mu_{ball.}$; note the temperature dependence. For the longest length scale selections, however, i.e., when L is set to 1 μm, the electron transport is dominated by the collision-dominated electron transport regime, $\mu_{ball.}$ becomes very large and $\mu_{eff.}$ essentially follows μ_{bulk}; once again, note the temperature dependence.

In order to assess the role of collision-dominated electron transport processes in comparison with their ballistic counterparts, drawing upon the scattering formalism of Chilleri *et al.*,[17,18] we introduce the collision-dominated fractional scattering (CDFS) parameter

$$\text{CDFS} \equiv \frac{\lambda_{bulk}}{\lambda_{cont.} + \lambda_{bulk}}, \tag{16}$$

this parameter quantifying the fraction of the total scattering that arises purely from bulk scattering processes, where $\lambda_{cont.}$ and λ_{bulk} are as previously defined; recall Eqs. (9) and (10). How close the CDFS parameter is to unity provides a sense as to how dominant collision-dominated scattering is. From Eqs. (9) and (10), it can be seen that

$$\text{CDFS} = \frac{\frac{1}{\mu_{bulk}}}{\frac{1}{\mu_{ball.}} + \frac{1}{\mu_{bulk}}}, \tag{17}$$

which, recalling Eq. (11), can be more succinctly expressed as

$$\text{CDFS} = \frac{\frac{1}{\mu_{bulk}}}{\frac{1}{\mu_{eff.}}}, \tag{18}$$

where μ_{bulk} and $\mu_{eff.}$ are as defined previously. The dependence of CDFS on both the length scale, L, and the crystal temperature, T, is

depicted in Figs. 4(a) and 4(b) for the cases of Si and GaAs, respectively. It is noted that as L is diminished that the CDFS parameter is reduced. The amount by which CDFS is reduced depends on how the ballistic mobility component, $\mu_{ball.}$, contrasts with that associated with the bulk, μ_{bulk}. The fact that the temperature dependence of μ_{bulk} is stronger than that associated with $\mu_{ball.}$ (recall Fig. 2) suggests that ballistic electron transport is going to be more dominant at the lower temperatures while it is going to be less significant at the higher temperatures, as is seen in Figs. 4(a) and 4(b).

V. COMPARISON WITH THE RESULTS OF EXPERIMENT

As a coda to this analysis, we now present a comparison with the results of experiment. Owing to limitations in the availability of

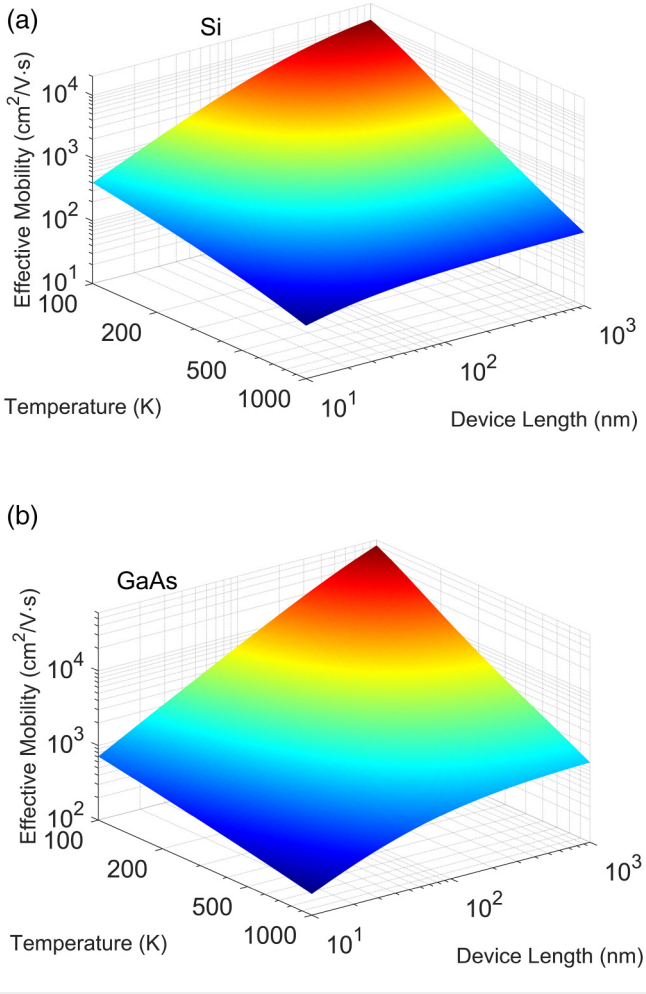

FIG. 3. (a) The effective mobility associated with Si, $\mu_{eff.}$, as a function of the length scale, L, and the crystal temperature, T. These results are determined through the use of Eq. (11), the bulk Si mobility component, μ_{bulk}, being determined from the bulk temperature dependence shown in Fig. 2(a). The Si $\mu_{ball.}$ value is determined through the use of Eqs. (8) and (13), m^* being set to the Si value prescribed in Table I. The online version of this figure is depicted in color. (b) The effective mobility associated with GaAs, $\mu_{eff.}$, as a function of the length scale, L, and the crystal temperature, T. These results are determined through the use of Eq. (11), the bulk GaAs mobility component, μ_{bulk}, being determined from the bulk temperature dependence shown in Fig. 2(b). The GaAs $\mu_{ball.}$ value is determined through the use of Eqs. (8) and (13), m^* being set to the GaAs value prescribed in Table I. The online version of this figure is depicted in color.

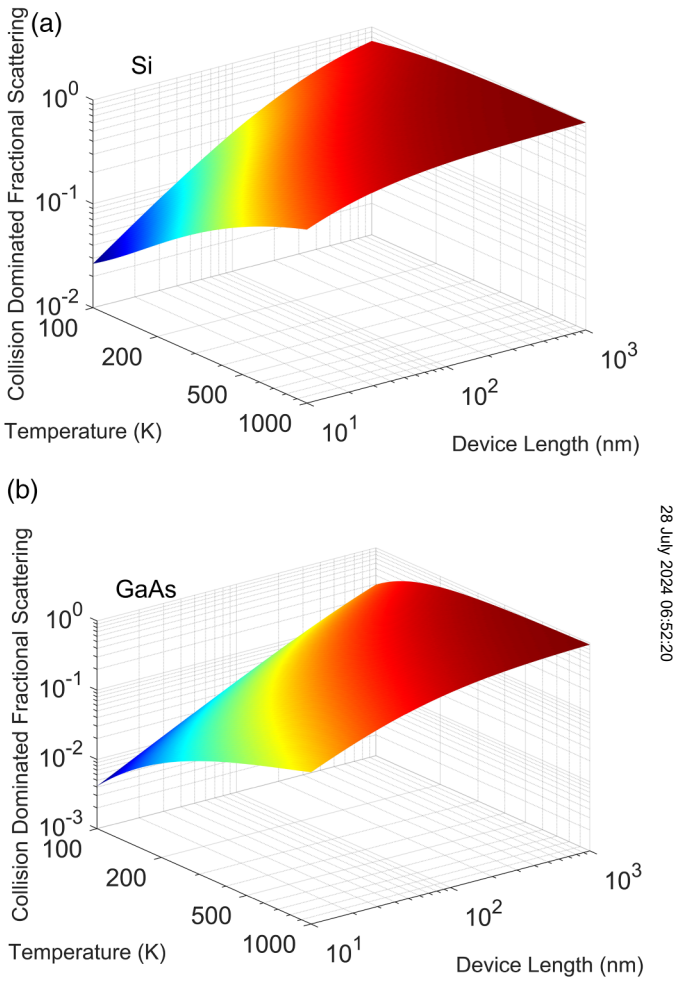

FIG. 4. (a) The CDFS parameter associated with Si, as a function of the length scale, L, and the crystal temperature, T. These results are determined through the use of Eq. (18), the bulk Si mobility component, μ_{bulk}, being determined from the temperature dependence shown in Fig. 2(a). The Si $\mu_{ball.}$ value is determined through the use of Eqs. (8) and (13), m^* being set to the Si value prescribed in Table I. The online version of this figure is depicted in color. (b) The CDFS parameter associated with GaAs, as a function of the length scale, L, and the crystal temperature, T. These results are determined through the use of Eq. (18), the bulk GaAs mobility component, μ_{bulk}, being determined from the temperature dependence shown in Fig. 2(b). The GaAs $\mu_{ball.}$ value is determined through the use of Eqs. (8) and (13), m^* being set to the GaAs value prescribed in Table I. The online version of this figure is depicted in color.

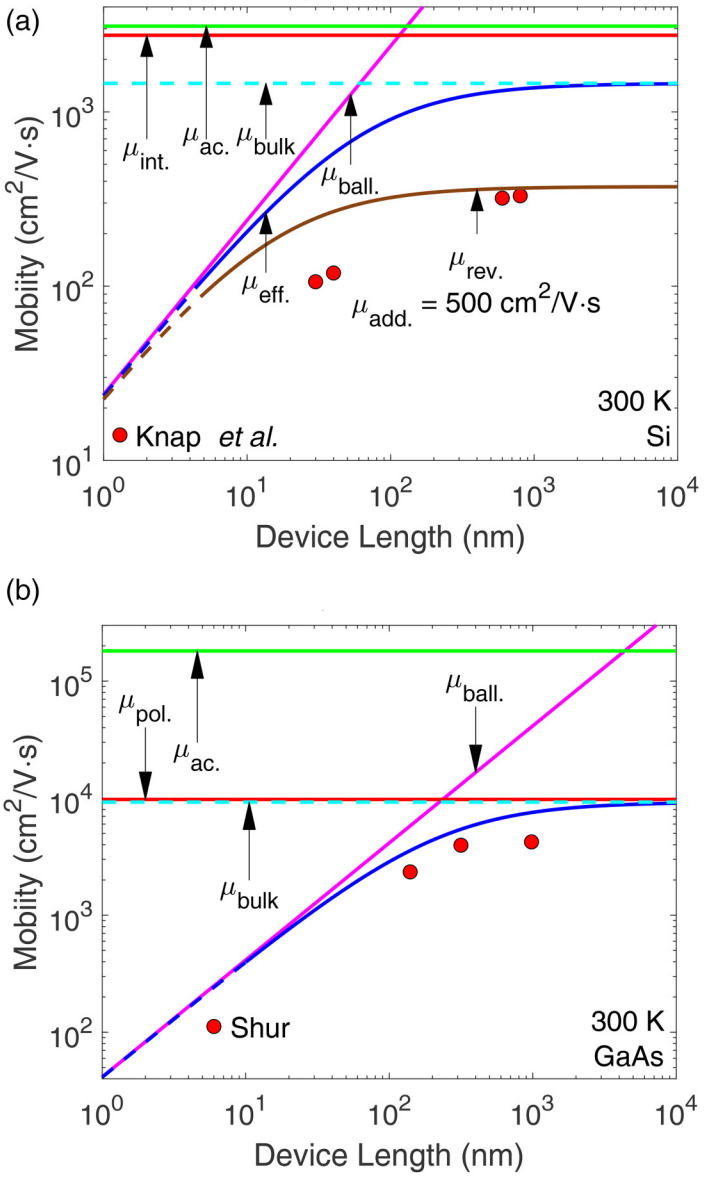

FIG. 5. (a) The effective mobility, $\mu_{eff.}$, plotted as a function of the device feature length scale, L, for the case of Si. The computed results are depicted with lines, solid lines being used for gate lengths greater than or equal to the 5 nm limit suggested by Kawaura *et al.*,[7] the extensions of the results to shorter gate lengths being rendered with the dashed lines. The crystal temperature is set to 300 K for these computations. The factors contributing to Si's bulk mobility, μ_{bulk}, i.e., the component of mobility related to inter-valley scattering, $\mu_{int.}$, and the component of mobility related to acoustic deformation potential scattering, $\mu_{ac.}$, are depicted, as is the resultant bulk mobility value, μ_{bulk}, this value being determined through the use of Eq. (14). The dependence of the ballistic mobility, $\mu_{ball.}$, on the length scale, L, is also depicted, the $\mu_{eff.}$ dependence on L being evaluated through the use of Eq. (11). The dependence of the revised effective mobility, $\mu_{rev.}$, on the device feature length scale, L, is also depicted, this result being determined through the use of Eq. (19), the additional mobility component, $\mu_{add.}$, being set to 500 $cm^2/V\,s$. The experimental results of Knap *et al.*[28] are depicted with the solid points. The online version of this figure is depicted in color. (b) The effective mobility, $\mu_{eff.}$, plotted as a function of the device feature length scale, L, for the case of GaAs. The computed results are depicted with lines, solid lines being used for gate lengths greater than or equal to a 10 nm limit, the extensions of the results to shorter gate lengths being rendered with the dashed lines; GaAs, being a less developed material system, as of yet at least, can not scale to the same level as Si. The crystal temperature is set to 300 K for these computations. The factors contributing to GaAs's bulk mobility, μ_{bulk}, i.e., the component of mobility related to polar optical phonon scattering, $\mu_{pol.}$, and the component of mobility related to acoustic deformation potential scattering, $\mu_{ac.}$, are depicted, as is the resultant bulk mobility value, μ_{bulk}, this value being determined through the use of Eq. (15). The dependence of the ballistic mobility, $\mu_{ball.}$, on the length scale, L, is also depicted, the $\mu_{eff.}$ dependence on L being evaluated through the use of Eq. (11). The experimental results reported by Shur[32] are depicted with the solid points. The online version of this figure is depicted in color.

relevant experimental data, we confine this comparison to the dependence of the effective mobility, $\mu_{\text{eff.}}$, on the length scale, L, the influence that crystal temperature plays in shaping $\mu_{\text{eff.}}$ for various length scale selections being experimentally unresolved at present.[27] We start the analysis with the case of Si, the experimental results of Knap *et al.*[28] providing the basis for comparison, these experimental results providing the dependence of the experimentally resolved mobility on the gate length for a series of Si-based transistors, the transistor gate lengths considered by Knap *et al.*[28] ranging between 30 and 800 nm. In Fig. 5(a), we plot the dependence of the effective mobility, $\mu_{\text{eff.}}$, on the length scale, L, the dependence of the ballistic mobility, $\mu_{\text{ball.}}$, also being depicted, a 300 K crystal temperature being assumed for the purposes of these computations. As a point of reference, the 300 K bulk mobility associated with Si, μ_{bulk}, determined through the use of Eq. (14), is also shown, the $\mu_{\text{int.}}$ and $\mu_{\text{ac.}}$ bulk Si mobility contributions being shown. The experimental results of Knap *et al.*[28] are also shown in Fig. 5(a), our interpretation being that the gate length values serve as a proxy for the length scale, L; of course, transiting electrons will not only transit directly across the length scale, some of the geometrical considerations being taken into account with the aforementioned averaging process.[29] It is noted that the computed $\mu_{\text{eff.}}$ forms a relatively wide upper bound to the experimental results of Knap *et al.*,[28] which might not have been unexpected considering that our computations of the low-field bulk mobility only take $\mu_{\text{int.}}$ and $\mu_{\text{ac.}}$ into account. Ionized impurity scattering, which has been neglected as we assumed intrinsic Si, could play an important role in determining the bulk mobility, μ_{bulk}, and could account for some of the differences that are seen; Jacoboni *et al.*[30] observe that at 300 K the electron mobility associated with bulk Si reduces to values lower than 500 $\text{cm}^2/\text{V s}$ for doping concentrations in excess of 10^{17} cm^{-3}. Non-bulk scattering processes, such as surface roughness scattering, are also likely to shape the results, particularly as the length scales become small, it being plausible that the relative impact of the surface roughness becomes greater as L becomes shorter; surface roughness limited mobility evaluations of the order of 1000 $\text{cm}^2/\text{V s}$ are found for the case of Si.[31] Adding in an additional scattering process into the electron transport calculus, the mobility associated with this particular process, $\mu_{\text{add.}}$, being set to 500 $\text{cm}^2/\text{V s}$, a revised effective mobility may then be determined, where the revised mobility, $\mu_{\text{rev.}}$, may be determined through the use of another Matthiessen's-rule based computation between $\mu_{\text{eff.}}$ and $\mu_{\text{add.}}$, i.e.,

$$\frac{1}{\mu_{\text{rev.}}} = \frac{1}{\mu_{\text{eff.}}} + \frac{1}{\mu_{\text{add.}}}, \tag{19}$$

where all terms in Eq. (19) are as previously defined; at this point, we are agnostic into the exact origins of this additional scattering process, but note that it represents a composite over the scattering processes that were neglected in the evaluation of $\mu_{\text{eff.}}$ itself. It is observed that $\mu_{\text{rev.}}$ forms a much tighter bound on the experimental data of Knap *et al.*[28] than that provided by $\mu_{\text{eff.}}$. Clearly, further analysis would be required in order to account for the differences observed.

We complete the analysis with the case of GaAs, the experimental results presented by Shur[32] providing the basis for comparison, these experimental results providing the dependence of the experimentally resolved mobility on the gate length for a series of GaAs-based transistors, the transistor gate lengths ranging between 150 and 1000 nm; note that the shortest gate length here is five times the shortest Si gate length considered in the experimental data set of Knap *et al.*[28] In Fig. 5(b), we plot the dependence of the effective mobility, $\mu_{\text{eff.}}$, on the length scale, L, the dependence of the ballistic mobility, $\mu_{\text{ball.}}$, also being depicted, a 300 K crystal temperature being assumed for the purposes of these computations. As a point of reference, the 300 K bulk mobility associated with GaAs, μ_{bulk}, determined through the use of Eq. (15), is also shown, the $\mu_{\text{pol.}}$ and $\mu_{\text{ac.}}$ bulk GaAs mobility contributions being indicated. The experimental results of Shur[32] are shown, our interpretation being that the gate length values serve as a proxy for the length scale, L. It is noted that the computed $\mu_{\text{eff.}}$ forms a relatively tight upper bound to the experimental results of Shur.[32] The small differences that are observed in this case are probably related to our lack of account of the ionized impurity scattering that is present, this being neglected as we assumed an intrinsic form of GaAs. The higher mobility values associated with GaAs compared with Si, for both the ballistic and bulk mobility components, and the fact that GaAs devices considered by Shur[32] are larger in scale than the Si devices considered by Knap *et al.*,[28] i.e., the relative impact of the surface roughness is smaller for these larger devices, possibly accounts for why the upper bound observed in Fig. 5(b) is tighter than that found in Fig. 5(a). Clearly, further work into this matter would be required in order to draw more definitive conclusions.

VI. CONCLUSIONS

In conclusion, building upon the scattering formalism of Chilleri *et al.*,[17,18] we have developed a means of quantitatively examining the transition between the collision-dominated and ballistic electron transport regimes in the electron transport "space" as the length scale is reduced. In order to place this transition on a continuum, we have introduced the CDFS parameter, this parameter quantifying the fraction of the scattering that arises purely from bulk scattering processes. Evaluations of the effective mobility, $\mu_{\text{eff.}}$, and the CDFS parameter are pursued for both materials of interest, these evaluations being performed as functions of the length scale, L, and the crystal temperature, T. Finally, for the sake of concreteness, we have compared the predictions of our analysis with room temperature experimental results for two conventional semiconductors of interest, Si and GaAs.

ACKNOWLEDGMENTS

The authors would like to acknowledge the Natural Sciences and Engineering Research Council of Canada and MITACS for financial support.

AUTHOR DECLARATIONS

Conflict of Interest

The authors have no conflicts to disclose.

Author Contributions

All of the computations were performed by Alireza Azimi, Mohammadreza Azimi, and Stephen K. O'Leary. All of the figures were produced by Alireza Azimi and Stephen K. O'Leary. The text was primarily written by Alireza Azimi and Stephen K. O'Leary, in consultation with Michael S. Shur. The work of Alireza Azimi and Mohammadreza Azimi was supervised by Stephen K. O'Leary. Michael S. Shur made some invaluable technical suggestions with respect to this manuscript, these helping shape its form and clarity.

Alireza Azimi: Conceptualization (lead); Formal analysis (lead); Investigation (lead); Methodology (lead); Validation (lead); Visualization (lead); Writing – original draft (lead); Writing – review & editing (lead). **Mohammadreza Azimi:** Formal analysis (equal); Methodology (equal); Writing – original draft (equal); Writing – review & editing (equal). **Michael S. Shur:** Conceptualization (equal); Writing – original draft (supporting). **Stephen K. O'Leary:** Conceptualization (equal); Formal analysis (equal); Funding acquisition (equal); Investigation (equal); Methodology (equal); Project administration (equal); Resources (equal); Supervision (equal); Visualization (equal); Writing – original draft (equal); Writing – review & editing (equal).

DATA AVAILABILITY

The data that support the findings of this study are available from the corresponding author upon reasonable request.

APPENDIX: THERMAL VELOCITY EVALUATION

For the case of two-dimensional electron transport, the non-degenerate electron distribution function may be expressed as

$$f(v_x, v_y) = \frac{m}{2\pi\, k_B T} \exp\left(-\frac{m^* v^2}{2k_B T}\right), \tag{A1}$$

where v denotes the velocity magnitude, i.e., $v = \sqrt{v_x^2 + v_y^2}$, v_x and v_y representing the two distinct electron velocity coordinates; the pre-factor of Eq. (A1) may be determined through the normalization condition, i.e.,

$$\int_{-\infty}^{\infty}\int_{-\infty}^{\infty} f(v_x, v_y)\, dv_x\, dv_y = 1. \tag{A2}$$

The thermal velocity may be evaluated by finding the average velocity magnitude over the ensemble, i.e.,

$$v_{\text{th.}} = \int_{-\infty}^{\infty}\int_{-\infty}^{\infty} v\, f(v_x, v_y)\, dv_x\, dv_y. \tag{A3}$$

Noting the radial symmetry embedded in $f(v_x, v_y)$, we convert our evaluation of $v_{\text{th.}}$ into radial coordinates, noting then that

$$v_{\text{th.}} = \left(\frac{m}{k_B T}\right)\int_0^{\infty} v^2 \exp\left(-\frac{m^* v^2}{2k_B T}\right) dv. \tag{A4}$$

which can be evaluated through integration-by-parts; such a process may be used to show that

$$\int_0^{\infty} v^2 \exp\left(-\frac{m^* v^2}{2k_B T}\right) dv = \frac{1}{\left(\frac{m}{k_B T}\right)}\int_0^{\infty} \exp\left(-\frac{m^* v^2}{2k_B T}\right) dv. \tag{A5}$$

From the conjuncture of Eqs. (A4) and (A5), observing that

$$\int_0^{\infty} \exp\left(-\frac{m^* v^2}{2k_B T}\right) dv = \sqrt{\frac{2k_B T}{m^*}}\frac{\sqrt{\pi}}{2}, \tag{A6}$$

we find that

$$v_{\text{th.}} = \sqrt{\frac{\pi k_B T}{2m^*}}, \tag{A7}$$

which exactly corresponds with Eq. (13).

REFERENCES

[1] M. Ieong, B. Doris, J. Kedzierski, K. Rim, and M. Yang, Science **306**, 2057 (2004).
[2] R. Chau, B. Doyle, S. Datta, J. Kavalieros, and K. Zhang, Nat. Mater. **6**, 810 (2007).
[3] A. B. Kelleher, "Celebrating 75 years of the transistor A look at the evolution of Moore's Law innovation," in *Technical Digest—International Electron Devices Meeting IEDM* (IEEE, 2022), p. 111.
[4] M. Radosavljevic and J. Kavalieros, IEEE Spectrum **59**, 32 (2022).
[5] M. Bohr, Commun. ACM **41**, 80 (1998).
[6] V. Passi and J.-P. Raskin, Semicond. Sci. Technol. **32**, 123004 (2017).
[7] H. Kawaura, T. Sakamoto, and T. Baba, Appl. Phys. Lett. **76**, 3810 (2000).
[8] S. B. Desai, S. R. Madhvapathy, A. B. Sachid, J. P. Llinas, Q. Wang, G. H. Ahn, G. Pitner, M. J. Kim, J. Bokor, C. Hu, H.-S. P. Wong, and A. Javey, Science **354**, 99 (2016).
[9] D.-M. Tang, S. V. Erohin, D. G. Kvashnin, V. A. Demin, O. Cretu, S. Jiang, L. Zhang, P.-X. Hou, G. Chen, D. N. Futaba, Y. Zheng, R. Xiang, X. Zhou, F.-C. Hsia, N. Kawamoto, M. Mitome, Y. Nemoto, F. Uesugi, M. Takeguchi, S. Maruyama, H.-M. Cheng, Y. Bando, C. Liu, P. B. Sorokin, and D. Golberg, Science **374**, 1616 (2021).
[10] M. S. Shur and L. F. Eastman, IEEE Trans. Electron Devices **26**, 1677 (1979).
[11] A. A. Kastalsky and M. S. Shur, Solid State Commun. **39**, 715 (1981).
[12] A. A. Kastalsky, M. S. Shur, and K. Lee, "Conductance of small semiconductor devices," in *Proceedings of 8th Biennial Cornell Electrical Engineering Conference* (1981).
[13] A. van der Ziel, M. S. Shur, K. Lee, T.-H. Chen, and K. Amberiadis, IEEE Trans. Electron Devices **30**, 128 (1983).
[14] A. P. Dmitriev and M. S. Shur, Appl. Phys. Lett. **89**, 142102 (2006).
[15] K. Lee and M. S. Shur, J. Appl. Phys. **54**, 4028 (1983).
[16] A. Azimi, M. Azimi, M. S. Shur, and S. K. O'Leary, J. Appl. Phys. **134**, 125701 (2023).
[17] J. Chilleri, Y. Wang, M. S. Shur, and S. K. O'Leary, Solid State Commun. **352**, 114776 (2022).
[18] J. Chilleri, Y. Wang, and S. K. O'Leary, Solid State Commun. **356**, 114925 (2022).
[19] A 2DEG can form in the immediate vicinity of a heterojunction, i.e., the interface between two dissimilar materials.
[20] M. Lundstrom, IEEE Electron Device Lett. **18**, 361 (1997).
[21] M. S. Lundstrom and J. Guo, *Nanoscale Transistors Device Physics, Modeling and Simulation* (Springer, New York, 2006).
[22] D. Antoniadis, IEEE Trans. Electron Devices **63**, 2650 (2016).

[23]Generalizations of this analysis for the "soft" contact case, when the probability of scattering at a device boundary is less than unity, brings our formalism into complete alignment with the spirit of the formalisms of Lundstrom[20,21] and Antoniadis.[22]
[24]J. Chilleri, P. Siddiqua, M. S. Shur, and S. K. O'Leary, Appl. Phys. Lett. **120**, 122105 (2022).
[25]D. L. Rode, Phys. Status Solidi (B) **53**, 245 (1972).
[26]M. Shur, B. Gelmont, and M. A. Khan, J. Electron. Mater. **25**, 777 (1996).
[27]For the purposes of this analysis, we neglect any screening length considerations on account of the fact that the screening lengths associated with the materials under consideration are, for the most part at least, relatively short when contrasted with the gate lengths considered in this comparative analysis; see Azimi *et al.*[16]
[28]W. Knap, F. Teppe, Y. Meziani, N. Dyakonova, J. Lusakowski, F. Boeuf, T. Skotnicki, D. Maude, S. Rumyantsev, and M. S. Shur, Appl. Phys. Lett. **85**, 675 (2004).
[29]We consider this approximation as sort of being analogous to the gradual channel approximation, an approximation often used in the modeling of field effect transistor behavior.
[30]C. Jacoboni, C. Canali, G. Ottaviani, and A. A. Quaranta, Solid–State Electron. **20**, 77 (1977).
[31]D. Lizzit, D. Esseni, P. Palestri, and L. Selmi, J. Appl. Phys. **116**, 223702 (2014).
[32]M. S. Shur, IEEE Electron Device Lett. **23**, 511 (2002).